OPTICS

Freeform direct-write and rewritable photonic integrated circuits in phase-change thin films

Changming Wu[1], Haoqin Deng[1], Yi-Siou Huang[2,3], Heshan Yu[2,4], Ichiro Takeuchi[2], Carlos A. Ríos Ocampo[2,3], Mo Li[1,5]*

Copyright © 2024 The Authors, some rights reserved; exclusive licensee American Association for the Advancement of Science. No claim to original U.S. Government Works. Distributed under a Creative Commons Attribution NonCommercial License 4.0 (CC BY-NC).

Photonic integrated circuits (PICs) with rapid prototyping and reprogramming capabilities promise revolutionary impacts on a plethora of photonic technologies. We report direct-write and rewritable photonic circuits on a low-loss phase-change material (PCM) thin film. Complete end-to-end PICs are directly laser-written in one step without additional fabrication processes, and any part of the circuit can be erased and rewritten, facilitating rapid design modification. We demonstrate the versatility of this technique for diverse applications, including an optical interconnect fabric for reconfigurable networking, a photonic crossbar array for optical computing, and a tunable optical filter for optical signal processing. By combining the programmability of the direct laser writing technique with PCM, our technique unlocks opportunities for programmable photonic networking, computing, and signal processing. Moreover, the rewritable photonic circuits enable rapid prototyping and testing in a convenient and cost-efficient manner, eliminate the need for nanofabrication facilities, and thus promote the proliferation of photonics research and education to a broader community.

INTRODUCTION

The application of photonic integrated circuits (PICs) is rapidly spreading in diverse technology domains, ranging from computing (*1*–*3*), communication (*4*–*6*), sensing (*7*–*9*), and quantum technology (*10*–*13*). Traditionally, PICs are fabricated in thin-film materials, including silicon (*4*, *14*, *15*), silicon nitride (*16*, *17*), indium phosphide (*18*, *19*), and lithium niobates (*20*, *21*), using top-down nanofabrication processes including lithography, etching, and deposition on tools installed in cleanroom facilities. Compared with electronics, where prototypes can be rapidly built by students using discrete elements plugged into a breadboard, photonics research faces the barriers of the limited accessibility to fabrication facilities, the high costs associated with the fabrication process, and the extended design-to-device turnaround time. The environmental impact and chemical waste generated by the top-down fabrication process of PICs are also a concern. The combination of these barriers impedes widespread innovation and throttles the broader impact of photonics research and education.

Moreover, there is a growing interest in programmable PICs to realize highly flexible photonic networks for emerging applications, including optical computing, optical interconnect for neural network accelerators (*15*, *22*–*24*), and quantum computing (*25*–*28*). Now, programmable PICs are realized through a network of tunable components, including phase shifters, directional couplers, and interferometers, connected in a highly complex architecture (*29*–*31*). The programmability of those schemes has been limited to switching and rerouting the network, while freeform reconfiguration of the system's functionality remains difficult to achieve. As the complexity increases, programmable PICs face overwhelming challenges of scalability, programming precision, and flexibility, which limit their practicality and increase cost (*32*–*34*).

Here, we report a simple, fast-turnaround, and low-cost approach to creating and reprogramming PICs that could shift the paradigm in photonics research, prototyping, and education. By eliminating the reliance on traditional fabrication processes, our technique enables researchers to explore a wider space of design possibilities and system functionalities more rapidly. Moreover, such a technique will allow researchers and students who do not have access to nanofabrication facilities to prototype and reuse PIC designs and thus democratize photonics research to a broader community. It will enable more students and educators to engage in hands-on experimentation, thereby fostering innovation and knowledge dissemination and generating a broader impact to promote workforce development in photonics.

Our technique is based on direct laser writing (DLW) on phase-change material (PCM) thin films. The method writes the PICs in only one optical patterning step and without using any traditional lithography and etching processes. The PICs are created by using PCM's marked refractive index contrast between the two nonvolatile phases, amorphous and crystalline, which are reversibly switchable using optical pulses (*35*). We have demonstrated direct writing of functional PICs consisting of a full package of building-block photonic components, including waveguides, gratings, ring resonators, couplers, crossings, and interferometers. These direct-write PICs are also rewritable, allowing convenient erasure and recreation of the circuits either partially or entirely, thereby completely changing their functionality to suit very different application scenarios.

Previously, laser writing to control phase transition in PCMs has been used in optical storage, such as rewritable compact disks (*35*). Free-space optical switching of PCMs has also been used to realize reconfigurable metasurface (*36*, *37*), programmable silicon photonics (*38*), rewritable color displays (*39*), and polariton nanophotonic devices (*40*). Laser patterning of photonic circuits has been reported, including femtosecond laser writing of waveguides in silica (*41*–*45*) and chalcogenide glasses (*46*–*48*) and a programmable III-V semiconductor-based photonic device (*49*). However, the photon-induced refractive index contrast for glass waveguide application is small, typically less than 0.1 (*46*–*48*). This limitation constrains not only the footprint of the devices but also their potential applications. On the other hand, optical

[1]Department of Electrical and Computer Engineering, University of Washington, Seattle, WA 98195, USA. [2]Department of Materials Science and Engineering, University of Maryland, College Park, MD 20742, USA. [3]Institute for Research in Electronics and Applied Physics, University of Maryland, College Park, MD 20742, USA. [4]School of Microelectronics, Tianjin University, Tianjin 300072, China. [5]Department of Physics, University of Washington, Seattle, WA 98195, USA.
*Corresponding author. Email: moli96@uw.edu

Downloaded from https://www.science.org at Stiftung Deutsches Elektronen-Synchrotron on January 23, 2024

patterning in III-V semiconductors is volatile, necessitating continuous laser irradiation for sustainability. In addition, none of the above techniques creates complete end-to-end PIC systems with multiple reconfigurable functions, as we report here.

RESULTS

Direct-write and rewritable PICs

Figure 1A illustrates the concept of direct writing, erasing, and rewriting PICs. The PIC is written on a standard oxidized silicon substrate, which is coated with a 200-nm-thick SiO_2 layer covering a 30-nm-thick Sb_2Se_3 layer on a 330-nm-thick Si_3N_4 film. The SiO_2 capping layer protects and prevents oxidation of the Sb_2Se_3 layer. Waveguiding in the Sb_2Se_3 film is achieved by using the crystalline phase (cSb_2Se_3) as the high-index core and the amorphous phase (aSb_2Se_3) as the cladding (Fig. 1B). This binary phase configuration, that is, no mixed phases, enables the confinement of the fundamental transverse electric (TE_0) optical mode within a cSb_2Se_3 waveguide, assisted by the underlayer of Si_3N_4, as shown in the simulated mode profile in Fig. 1C. We directly write the circuit layout on a blank cSb_2Se_3 thin film using a commercial laser writing system (Heidelberg DWL 66+, 405-nm laser), mainly to leverage its precision stage and computer control system for large-area writing. Alternatively, a homebuilt system using an off-the-shelf laser diode is sufficient to write a smaller area (note S2). To write the PICs, the focused laser beam with a power of 27.5 mW is scanned across the film at a speed of 3.0 mm^2/min, inducing a controlled phase transition from cSb_2Se_3 to aSb_2Se_3 (note S2) to create the claddings and define the core. This laser-controlled phase transition creates a circuit with a resolution limited by optical diffraction. Figure 1D shows a series of rectangular aSb_2Se_3 structures created by DLW with varying widths ranging from 1 μm to 200 nm. The minimum achievable feature size is 300 nm, exceeding the resolution reported in previous works (*37*–*40*). Moreover, the circuit layout can be erased either locally or globally. Local erasure is achieved by scanning the laser beam at a lower speed (0.1 mm^2/min) with a reduced laser power of 15 mW, inducing a phase transition from aSb_2Se_3 back to cSb_2Se_3 in desired areas (Fig. 1E). This capability enables modifications and corrections to the PIC design. Alternatively, global erasure can be accomplished by heating the whole substrate to above 180°C, promoting a complete phase transition across the entire PCM film. Thereby, the DLW technique provides very versatile capabilities for writing and rewriting phase-change PICs in freeform without using any advanced fabrication tools.

Direct-write PIC components

We first demonstrate the DLW of high-quality building-block components of PICs. The first example (Fig. 2A) is a racetrack ring resonator coupled with a bus waveguide connected to input and output grating couplers, all directly written with DLW. The resonator has a width of 1.2 μm and a radius of 120 μm with a gap of 350 nm to the bus waveguide (Fig. 2B). The pair of grating couplers couple light from optical fibers into the bus waveguide (Fig. 2C) with an efficiency of −14 dB. Figure 2D shows the measured transmission spectrum through the bus waveguide, showing the resonances of the ring resonator with an intrinsic quality factor is Q_i ~ 12,700, corresponding to a propagation loss of 2.8 dB mm^{-1}. The loss in the cSb_2Se_3 waveguide is mainly attributed to the scattering induced by the grain boundaries in the waveguide, as in-plane crystalline grains within the cSb_2Se_3 region can be observed with high-resolution electron microscopy (note S3). These grains, typically a few micrometers in size, are also randomly oriented (*50*). Because of the optical birefringence of cSb_2Se_3 (*39*), these randomly oriented grains result in the uneven absorption of laser energy during the DLW and limit the smoothness of the waveguide. The scattering loss can be mitigated when a lower erasure temperature is used to form larger crystal grains with sizes on the order of tens of micrometers, which we have observed. Further mitigation of the loss will require improved optical PCMs with finer polycrystalline structures. Nevertheless, the propagation loss of the cSb_2Se_3 waveguide is consistent with the reported values of dielectric waveguides integrated with Sb_2Se_3 (*50*–*53*).

The devices written on phase-change thin film exhibit consistent and reliable performance. To demonstrate this, we write multiple Mach-Zehnder interferometers (MZIs) with varied path length differences, ΔL, between the two arms (Fig. 2E). The measured transmission spectrum is shown in Fig. 2F. The consistently high extinction ratio (>20 dB) indicates that the 50/50 beam splitters (Fig. 2E, inset)

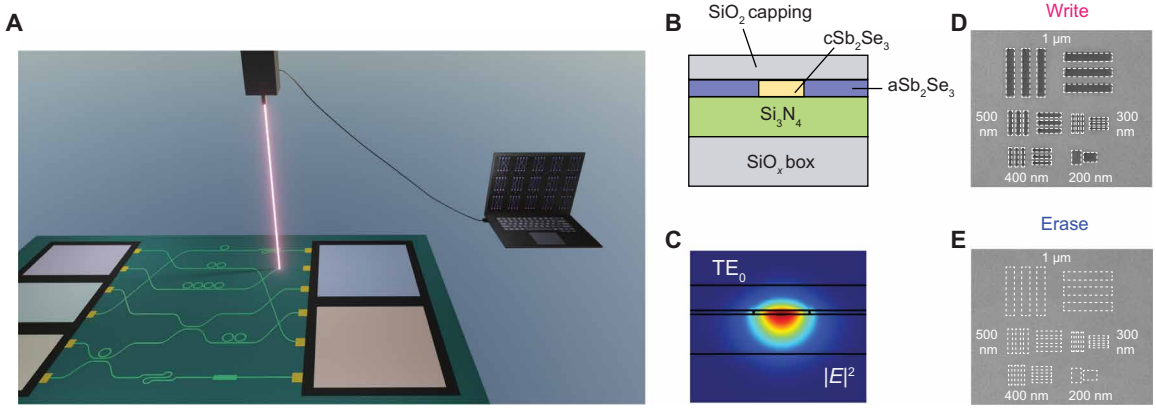

Fig. 1. Direct-write and rewritable phase-change photonic integrated circuits. (**A**) Artistic illustration of freeform writing and rewriting PICs on Sb_2Se_3 thin film. (**B**) The cross-sectional view of a cSb_2Se_3 optical waveguide structure. The waveguide is directly written in the PCM thin film without fabrication processes. (**C**) The simulated $|E|^2$ profile of the TE_0 mode in a cSb_2Se_3 waveguide, which is 1.2 μm wide and 30 nm thick, sits on top of a 330-nm-thick Si_3N_4-on-insulator substrate, and is capped with a 200-nm-thick SiO_2 for protection. (**D**) Optical image of aSb_2Se_3 resolution test patterns written on cSb_2Se_3 thin film. The minimum feature size achieved is 300 nm. (**E**) The same test pattern as in (D) is erased back to cSb_2Se_3.

Downloaded from https://www.science.org at Stiftung Deutsches Elektronen-Synchrotron on January 23, 2024

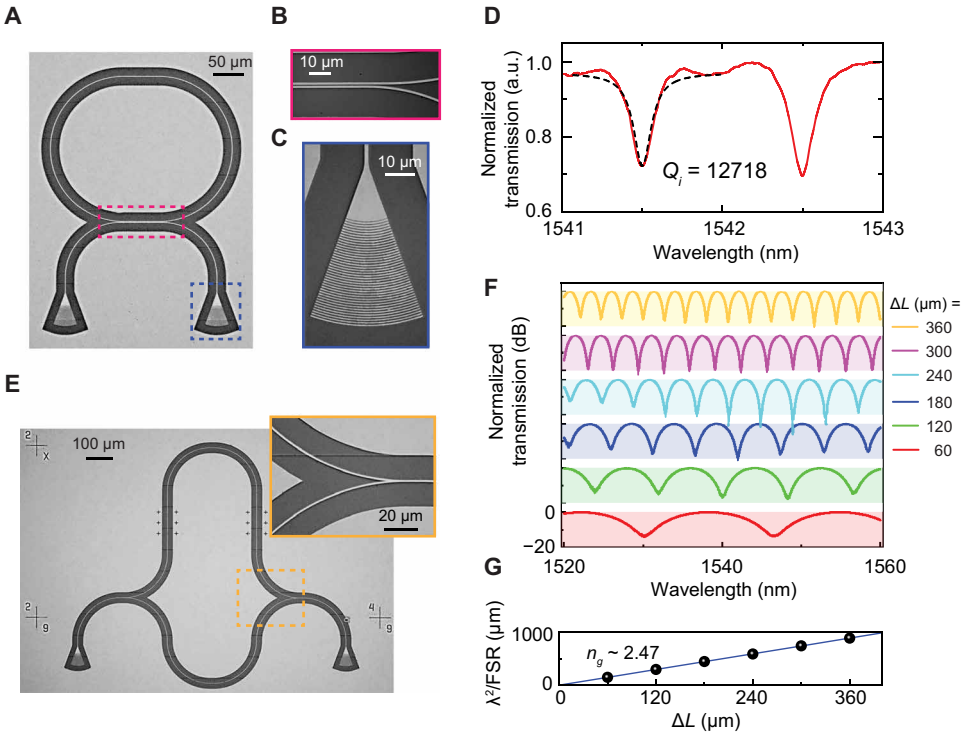

Fig. 2. Direct-write photonic components and their characterization. (**A**) Optical image of a racetrack ring resonator that is directly written on the Sb_2Se_3 thin film. (**B** and **C**) The zoomed-in optical image of the waveguide-ring coupling region (B) and the grating coupler (C). (**D**) The transmission spectrum of the ring resonator as shown in (A). The spectrum is normalized to the spectrum of a pristine Sb_2Se_3 waveguide. The intrinsic *Q* factor is 12,718. (**E**) Optical image of a direct-write PCM MZI. Inset: The zoomed-in image of the Y-combiner part in the MZI. (**F**) Normalized transmission spectra of the MZIs. Spectra have been vertically offset for clarity. (**G**) λ^2/free spectral range versus the length difference between two arms of the MZI, ΔL. Linear fitting yields a waveguide group index n_g of 2.47. a.u., arbitrary units.

perform very well. Fitting the spectra, we extract a group index $n_g = 2.47$ for a 1.2-μm-wide Sb_2Se_3 waveguide, which agrees well with the simulated value of 2.43. The characterization of other photonic building block elements, including directional couplers, waveguide crossings, and inverse-designed bends with low loss, are included in note S4.

Programmable interconnect fabric and crossbar matrix

Programmable optical interconnect fabric is a crucial photonic architecture to enable reconfigurable connectivity in telecommunication, computing, and network systems (*54*, *55*). Using the DLW technique, we can create and, on demand, route and reroute such interconnect fabric. In Fig. 3 (A to C), we demonstrate a 3 × 3 array, which establishes connectivity between three input and output ports using cSb_2Se_3 waveguides. We define the connection configuration of the fabric using a transmission matrix **M** in $S_{out} = \mathbf{M} \cdot S_{in}$, where S_{out} and S_{in} represent the output and input intensity vectors, respectively. As shown in Fig. 3A, we initially patterned the fabric to connect input/output ports in a configuration of 1 → 2, 2 → 1, and 3 → 3. The measurement result of this transmission matrix **M** shows that the extinction ratio between desired and undesired connections exceeds 20 dB (Fig. 3D). We then reroute the fabric by erasing all the waveguides in the designated connection region (Fig. 3B) and subsequently rewriting the waveguides to establish new connections with an updated configuration. As illustrated in Fig.3C, we reroute the switch array to the configuration of 1 → 2, 2 → 3, and 3 → 1. The measured **M** has changed accordingly but maintains a high extinction ratio > 18 dB. More data on routing and rerouting the optical fabric with other connection configurations can be found in note S6. In addition, we observe a residual image from the previous writing even after completely erasing the pattern. The residual image does not affect the performance of the newly patterned devices, though. We argue that this residual imprint can be explained by the optical birefringence resulting from size and orientation variations in cSb_2Se_3 crystal grains during the annealing processes. Specifically, during the laser erasing process, the crystal grains grow in alignment with the moving direction of the laser spot, while no preferred growth direction is present during the thermal erasing process (*50*).

A more complicated transmission matrix can be achieved by using a photonic crossbar array, which is a universal architecture for implementing multiply-accumulate (MAC) operation in linear optical computing (*56*, *57*). Figure 3F displays the optical image of a 14 × 14 photonic crossbar array written on the PCM thin film. As proof of concept, we demonstrate the operation of a 3 × 3 subarray to represent a programmable MAC core. The input vector is encoded by the intensities of optical signals in multiple wavelength channels, which are sent into each row of the crossbar array. As illustrated in Fig. 3G, each unit cell of the crossbar array consists of a row waveguide, a column waveguide, and a cross-coupling waveguide, which extracts the input signal from the row waveguide and couples it to the column waveguide through optimized directional couplers. Note S4 provides data on the splitting ratio of the directional coupler with various coupling lengths. The output of each column waveguide is the weighted sum of the input signal at each row and is measured incoherently by a photodetector,

Downloaded from https://www.science.org at Stiftung Deutsches Elektronen-Synchrotron on January 23, 2024

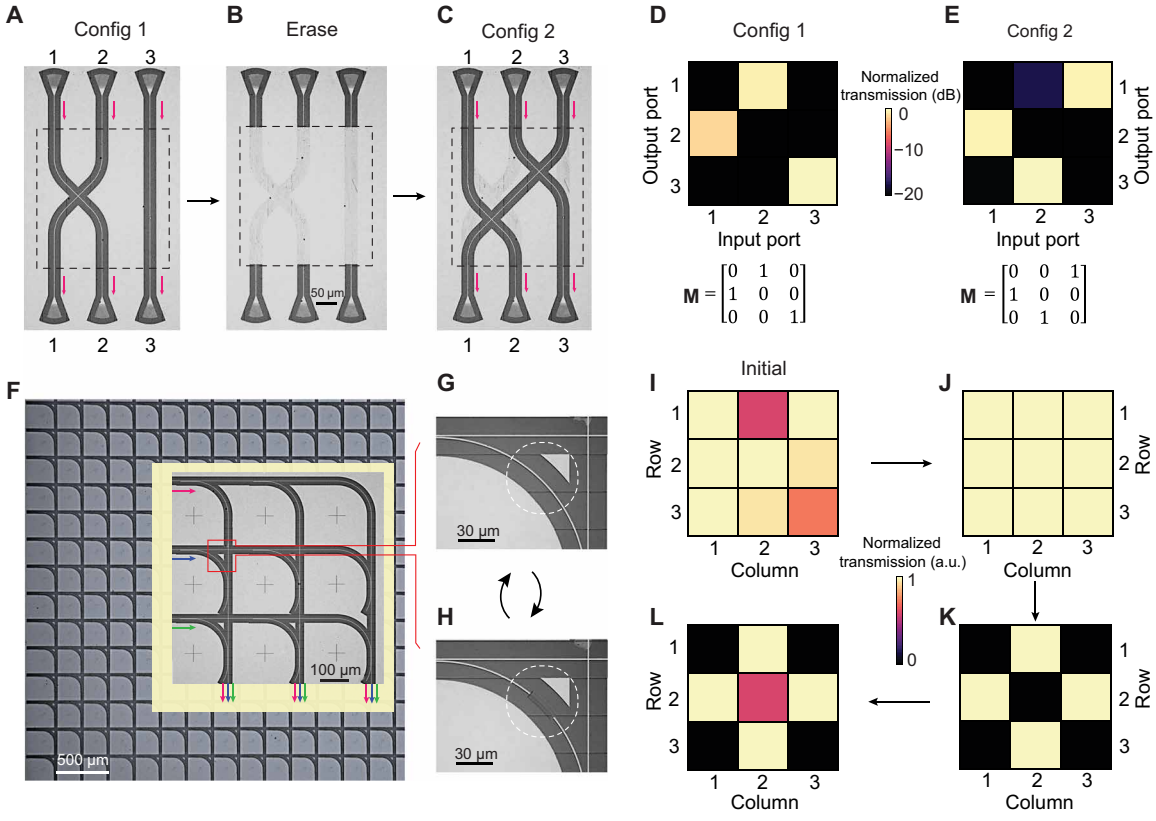

Fig. 3. Programmable photonic switch array and crossbar array. (**A**) Optical image of a 3 × 3 optical switch array with the initial connection configuration (matrix 1). The connection region of the optical switch is then erased (**B**) and rewritten (**C**) into a new connection configuration (matrix 2). (**D** and **E**) The measured transmission matrix of switch 1 (D) and switch 2 (E). (**F**) Optical image of a DLW 14 × 14 crossbar array. Inset: The 3 × 3 subarray used for testing. To decrease or increase the transmission of a specific crossbar element, the cross-coupling waveguide is partially erased (**H**) or recovered (**G**), respectively. (**I** and **J**) The transmission matrix of the crossbar array before and after correction. The crossbar array is initially designed to equally distribute the input power into outputs. Because of writing imperfections, the transmission matrix of the crossbar array has errors (I) and is corrected by DLW to restore the designed functionality (J). (**K** and **L**) Transmission matrix after setting the element at the center and four corners to 0 (K) and then resetting the center matrix element to 0.5 (L).

thus performing the MAC operation for matrix-vector multiplication. Each matrix element is programmed in the transmission of each unit cell's cross-coupling waveguide (see Fig. 3F). The output vector is obtained by measuring the total output power in each column of the output channels. A more detailed elucidation of crossbar array implementation can be found in previous works (*56*, *57*).

For demonstration, we initially designed and direct-wrote the 3 × 3 crossbar array to equally distribute the input power into the output to represent the matrix $\begin{bmatrix} 1 & 1 & 1 \\ 1 & 1 & 1 \\ 1 & 1 & 1 \end{bmatrix}$. However, because of writing imperfections (similar to fabrication variation in conventional PICs), the matrix represented by the crossbar array exhibits errors, as shown in the measured results in Fig. 3I. The DLW technique makes it straightforward to adjust each element by locally modifying the cross-coupling waveguides, thereby correcting the error to restore the designed functionality (Fig. 3J). It is also easy to reprogram the matrix in a grayscale-like fashion by erasing or restoring a section of the cross-coupling waveguide. As an example, we can set the element at the center and four corners to 0 (Fig. 3K) and decrease the center matrix element to 0.5 (Fig. 3L) to represent the matrix $\begin{bmatrix} 0 & 1 & 0 \\ 1 & 0.5 & 1 \\ 0 & 1 & 0 \end{bmatrix}$. Further data on tuning the attenuation and phase response of the Sb_2Se_3 waveguide can be found in note S5.

Shaping spectral response of coherent PICs

Coherent PICs universally use interferometric and resonant components and require precise spectral responses for filtering and coherent signal processing (*58*–*60*). Because of inevitable fabrication imprecision, it is necessary to shape these components' spectral responses to meet these requirements. The DLW technique allows us to incrementally trim the spectral response of a coherent optical filter step by step, offering a highly controlled method for fine-tuning its performance. In addition, we can even add new coherent components to change the spectral response entirely. As shown in Fig. 4A, we first write an MZI, which has a typical transmission spectral response as measured in Fig. 4G. We then erase a section of the lower arm of the MZI (Fig. 4B) and subsequently restore it and add a racetrack ring resonator, as depicted in Fig. 4C. The resulting transmission spectrum of the ring-coupled MZI displays features the characteristics of both the MZI and the ring resonator. Afterward, we erase portions of both the ring

Downloaded from https://www.science.org at Stiftung Deutsches Elektronen-Synchrotron on January 23, 2024

resonator and the MZI (see Fig. 4D) and rewrite the circuit to a double-injection ring (DIR) filter (*61*). In the DIR, the output light consists of cumulative contributions from two nominally identical add-drop ring resonators. The first contribution comes from the drop-port of the ring, with the input light incident from the lower arm of the original MZI. The second contribution originates from the through-port of the ring, with the light incident from the upper arm of the original MZI. As a result, the DIR exhibits a substantially different transmission spectrum with a much larger free spectral range (Fig. 4G). Last, we can trim the DIR spectral response by modifying its parameters. We adjust the coupling between the output waveguide and the racetrack ring resonators. This is done by widening the gap between the waveguides from 350 to 500 nm and reducing the waveguide width (Fig. 4F). The transmission spectrum of the modified DIR (DIR2 in Fig. 4F) changes as expected, thus demonstrating the spectral tunability of the filter. We note that all measured spectra from the filter agree well with the numerical models (further details are provided in note S7). This provides additional evidence of the stability and reliability of writing and rewriting the phase-change photonic circuits.

DISCUSSION

In conclusion, we have presented a flexible, reliable, and cost-effective technique for directly writing and rewriting photonic circuits on low-loss phase-change thin films. This technique simplifies the complex nanofabrication processes typically required for fabricating integrated photonic devices down to one-step laser writing and enables reusing the same chip/die. Although we have used a commercial laser writer in this work, we emphasize that the same results can be achieved with a much lower-cost laser writing system, which incorporates a laser diode, a focusing objective, a high-precision motion stage, and a computer control system (refer to note S2 for further information). This approach leverages the versatility of the DLW and the nonvolatile, low-loss, and high-contrast properties of the PCM, offering an unprecedented level of flexibility. We have demonstrated PICs consisting of a full package of elementary photonic components, including waveguides, grating couplers, ring resonators, MZIs, programmable optical switch fabrics, reconfigurable photonic crossbar array, and tunable optical filters. Although our demonstrations have been conducted in a near–in situ fashion, in steps of writing, measuring, modifying, and checking, real-time reconfiguration and feedback-controlled adaptation (*6*, *30*, *49*, *62*) of the PICs are entirely feasible.

Furthermore, the application scenario can be expanded by introducing a multilevel grayscale design (*37*, *39*, *57*, *63*–*65*) instead of the current binary design or by selecting appropriate substrates tailored to specific applications. For example, the phase-change thin films can also be integrated on $LiNbO_3$-on-insulator substrates, enabling the development of programmable electro-optical or acoustic-optical circuits. These advantages underscore the potential of the DLW technique in enabling the rapid prototyping and testing of innovative photonic circuits using only a low-cost tool that is affordable to a wide range of research and education communities.

MATERIALS AND METHODS

Substrate preparation

To prepare the substrate for DLW, a 30-nm-thick Sb_2Se_3 thin film sputtered on a 330-nm-thick Si_3N_4 on an oxidized silicon substrate at

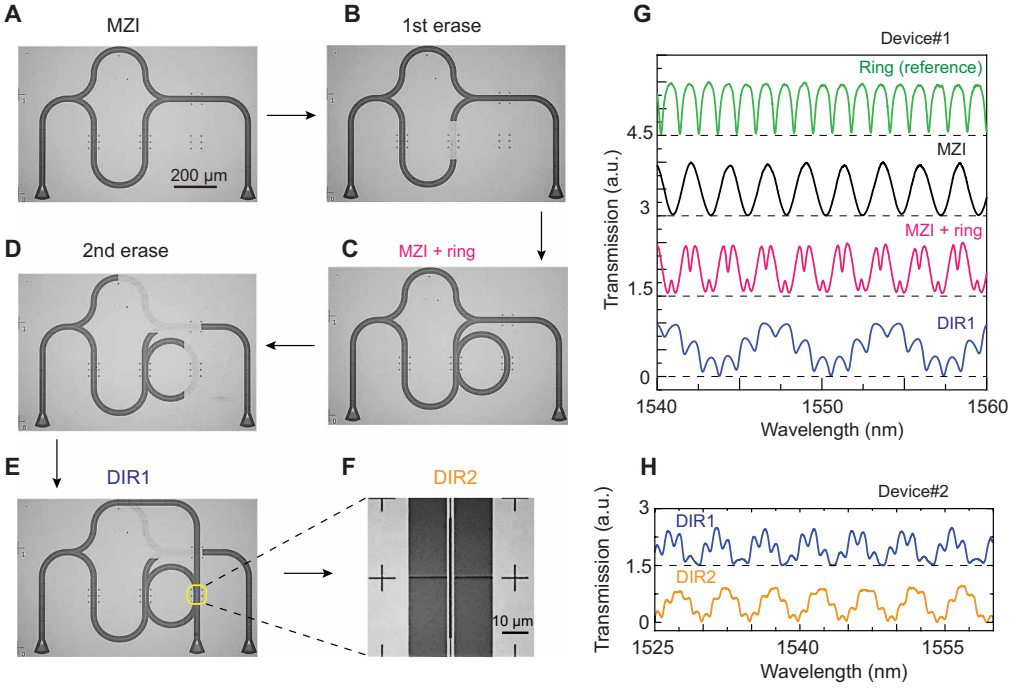

Fig. 4. Shaping the spectral response of an optical filter in steps. (**A**) An MZI written by DLW on a Sb_2Se_3 thin film. (**B**) Erase part of the bottom arm of the MZI. (**C**) Add a ring resonator to the erased region of the MZI. (**D**) Erase part of the ring resonator and the MZI. (**E**) Reconnect the device as the DIR filter. (**F**) Tuning the coupling by increasing the gap between the ring resonator and the top arm of the Y-splitter. (**G**) The transmission spectra of the optical filter after each reconfiguration step. Spectra have been vertically translated for clarity. (**H**) The transmission spectra of the DIR filter before (blue curve) and after (orange curve) tuning the ring resonator coupling.

Downloaded from https://www.science.org at Stiftung Deutsches Elektronen-Synchrotron on January 23, 2024

room temperature. The whole substrate was then capped with a 200-nm-thick SiO_2 for protection. After these two steps, the substrate was ready for laser writing.

Laser writing setup

We use a commercial 405-nm direct-writing lithography tool (Heidelberg DWL66+ with its Hires laser head) for the writing of the phase-change PICs. The laser power is set to 27.5 mW with a scanning speed of 3 mm^2/min. In addition, a homebuilt laser writing system is also applied to locally tune, erase, and rewrite the PICs (see fig. S3). In the homebuilt system, a 637-nm laser diode with a maximum output power of 170 mW (HL63133DG) is focused onto the substrate using a 50× objective lens with a numerical aperture of 0.55. To write a single spot, a rectangular pulse of 200-ns pulse duration and pulse energy of 50 nJ is used. To erase a single spot, the pulse duration is set to 5 ms with a pulse energy of 333 μJ. The sample was mounted on a two-dimensional *x-y* closed-loop motion stage, capable of a minimum moving step size of 50 nm. By synchronizing the controlled light pulse with the movement of the substrate on the stage, the desired pattern can be achieved. More details on the optical setup can be found in note S2.

Supplementary Materials

This PDF file includes:

Notes S1 and S7
Figs. S1 to S16
Tables S1 to S4

REFERENCES AND NOTES

1. C. Ríos, N. Youngblood, Z. Cheng, M. Le Gallo, W. H. P. Pernice, C. D. Wright, A. Sebastian, H. Bhaskaran, In-memory computing on a photonic platform. *Sci. Adv.* **5**, eaau5759 (2019).
2. X. Y. Xu, X. L. Huang, Z. M. Li, J. Gao, Z. Q. Jiao, Y. Wang, R. J. Ren, H. P. Zhang, X. M. Jin, A scalable photonic computer solving the subset sum problem. *Sci. Adv.* **6**, eaay5853 (2020).
3. Z. Ying, C. Feng, Z. Zhao, S. Dhar, H. Dalir, J. Gu, Y. Cheng, R. Soref, D. Z. Pan, R. T. Chen, Electronic-photonic arithmetic logic unit for high-speed computing. *Nat. Commun.* **11**, 2154 (2020).
4. A. H. Atabaki, S. Moazeni, F. Pavanello, H. Gevorgyan, J. Notaros, L. Alloatti, M. T. Wade, C. Sun, S. A. Kruger, H. Meng, K. Al Qubaisi, I. Wang, B. Zhang, A. Khilo, C. V. Baiocco, M. A. Popović, V. M. Stojanović, R. J. Ram, Integrating photonics with silicon nanoelectronics for the next generation of systems on a chip. *Nature* **556**, 349–354 (2018).
5. K. Y. Yang, C. Shirpurkar, A. D. White, J. Zang, L. Chang, F. Ashtiani, M. A. Guidry, D. M. Lukin, S. V. Pericherla, J. Yang, H. Kwon, J. Lu, G. H. Ahn, K. Van Gasse, Y. Jin, S. P. Yu, T. C. Briles, J. R. Stone, D. R. Carlson, H. Song, K. Zou, H. Zhou, K. Pang, H. Hao, L. Trask, M. Li, A. Netherton, L. Rechtman, J. S. Stone, J. L. Skarda, L. Su, D. Vercruysse, J. P. W. MacLean, S. Aghaeimeibodi, M. J. Li, D. A. B. Miller, D. M. Marom, A. E. Willner, J. E. Bowers, S. B. Papp, P. J. Delfyett, F. Aflatouni, J. Vučković, Multi-dimensional data transmission using inverse-designed silicon photonics and microcombs. *Nat. Commun.* **13**, 1–9 (2022).
6. X. Xu, G. Ren, T. Feleppa, X. Liu, A. Boes, A. Mitchell, A. J. Lowery, Self-calibrating programmable photonic integrated circuits. *Nat Photonics.* **16**, 595–602 (2022).
7. A. Z. Subramanian, E. Ryckeboer, A. Dhakal, F. Peyskens, A. Malik, B. Kuyken, H. Zhao, S. Pathak, A. Ruocco, A. De Groote, P. Wuytens, D. Martens, F. Leo, W. Xie, U. D. Dave, M. Muneeb, P. Van Dorpe, J. Van Campenhout, W. Bogaerts, P. Bienstman, N. Le Thomas, D. Van Thourhout, Z. Hens, G. Roelkens, R. Baets, Silicon and silicon nitride photonic circuits for spectroscopic sensing on-a-chip [Invited]. *Photonics Res.* **3**, B47 (2015).
8. E. Luan, H. Shoman, D. M. Ratner, K. C. Cheung, L. Chrowstowski, Silicon photonic biosensors using label-free detection. *Sensors.* **18**, 1–42 (2018).
9. S. Gyger, J. Zichi, L. Schweickert, A. W. Elshaari, S. Steinhauer, S. F. Covre da Silva, A. Rastelli, V. Zwiller, K. D. Jöns, C. Errando-Herranz, Reconfigurable photonics with on-chip single-photon detectors. *Nat. Commun.* **12**, 1–8 (2021).
10. G. Zhang, J. Y. Haw, H. Cai, F. Xu, S. M. Assad, J. F. Fitzsimons, X. Zhou, Y. Zhang, S. Yu, J. Wu, W. Ser, L. C. Kwek, A. Q. Liu, An integrated silicon photonic chip platform for continuous-variable quantum key distribution. *Nat Photonics.* **13**, 839–842 (2019).
11. J. Wang, F. Sciarrino, A. Laing, M. G. Thompson, Integrated photonic quantum technologies. *Nat Photonics.* **14**, 273–284 (2020).
12. X. Qiang, Y. Wang, S. Xue, R. Ge, L. Chen, Y. Liu, A. Huang, X. Fu, P. Xu, T. Yi, F. Xu, M. Deng, J. B. Wang, J. D. A. Meinecke, J. C. F. Matthews, X. Cai, X. Yang, J. Wu, Implementing graph-theoretic quantum algorithms on a silicon photonic quantum walk processor. *Sci. Adv.* **7**, 1–10 (2021).
13. X. Cheng, K. C. Chang, Z. Xie, M. C. Sarihan, Y. S. Lee, Y. Li, X. A. Xu, A. K. Vinod, S. Kocaman, M. Yu, P. G. Q. Lo, D. L. Kwong, J. H. Shapiro, F. N. C. Wong, C. W. Wong, A chip-scale polarization-spatial-momentum quantum SWAP gate in silicon nanophotonics. *Nat Photonics* **17**, 656–665 (2023).
14. C. Rogers, A. Y. Piggott, D. J. Thomson, R. F. Wiser, I. E. Opris, S. A. Fortune, A. J. Compston, A. Gondarenko, F. Meng, X. Chen, G. T. Reed, R. Nicolaescu, A universal 3D imaging sensor on a silicon photonics platform. *Nature* **590**, 256–261 (2021).
15. F. Ashtiani, A. J. Geers, F. Aflatouni, An on-chip photonic deep neural network for image classification. *Nature* **606**, 501–506 (2022).
16. M. Churaev, R. N. Wang, V. Snigirev, A. Riedhauser, T. Blésin, C. Möhl, M. A. Anderson, A. Siddharth, Y. Popoff, D. Caimi, S. Hönl, J. Riemensberger, J. Liu, P. Seidler, T. J. Kippenberg, A heterogeneously integrated lithium niobate-on-silicon nitride photonic platform. *Nat. Commun.* **1**, 3499 (2021).
17. J. Liu, G. Huang, R. N. Wang, J. He, A. S. Raja, T. Liu, N. J. Engelsen, T. J. Kippenberg, High-yield, wafer-scale fabrication of ultralow-loss, dispersion-engineered silicon nitride photonic circuits. *Nat. Commun.* **12**, 1–9 (2021).
18. R. Nagarajan, M. Kato, J. Pleumeekers, P. Evans, S. Corzine, S. Hurtt, A. Dentai, S. Murthy, M. Missey, R. Muthiah, R. A. Salvatore, C. Joyner, R. Schneider, M. Ziari, F. Kish, D. Welch, InP photonic integrated circuits. *IEEE J. Sel. Top. Quant. Electron.* **16**, 1113–1125 (2010).
19. L. M. Augustin, R. Santos, E. Den Haan, S. Kleijn, P. J. A. Thijs, S. Latkowski, D. Zhao, W. Yao, J. Bolk, H. Ambrosius, S. Mingaleev, A. Richter, A. Bakker, T. Korthorst, InP-based generic foundry platform for photonic integrated circuits. *IEEE J. Sel. Top. Quant. Electron.* **24**, 1–10 (2018).
20. C. Wang, M. Zhang, X. Chen, M. Bertrand, A. Shams-Ansari, S. Chandrasekhar, P. Winzer, M. Lončar, Integrated lithium niobate electro-optic modulators operating at CMOS-compatible voltages. *Nature* **562**, 101–104 (2018).
21. D. Zhu, L. Shao, M. Yu, R. Cheng, B. Desiatov, C. J. Xin, Y. Hu, J. Holzgrafe, S. Ghosh, A. Shams-Ansari, E. Puma, N. Sinclair, C. Reimer, M. Zhang, M. Lončar, Integrated photonics on thin-film lithium niobate. *Adv. Opt. Photonics.* **13**, 242–352 (2021).
22. Y. Shen, N. C. Harris, S. Skirlo, M. Prabhu, T. Baehr-Jones, M. Hochberg, X. Sun, S. Zhao, H. Larochelle, D. Englund, M. Soljacic, Deep learning with coherent nanophotonic circuits. *Nat Photonics.* **11**, 441–446 (2017).
23. B. J. Shastri, A. N. Tait, T. Ferreira de Lima, W. H. P. Pernice, H. Bhaskaran, C. D. Wright, P. R. Prucnal, Photonics for artificial intelligence and neuromorphic computing. *Nat Photonics.* **15**, 102–114 (2021).
24. H. H. Zhu, J. Zou, H. Zhang, Y. Z. Shi, S. B. Luo, N. Wang, H. Cai, L. X. Wan, B. Wang, X. D. Jiang, J. Thompson, X. S. Luo, X. H. Zhou, L. M. Xiao, W. Huang, L. Patrick, M. Gu, L. C. Kwek, A. Q. Liu, Space-efficient optical computing with an integrated chip diffractive neural network. *Nat. Commun.* **13**, 1–9 (2022).
25. X. Qiang, X. Zhou, J. Wang, C. M. Wilkes, T. Loke, S. O'Gara, L. Kling, G. D. Marshall, R. Santagati, T. C. Ralph, J. B. Wang, J. L. O'Brien, M. G. Thompson, J. C. F. Matthews, Large-scale silicon quantum photonics implementing arbitrary two-qubit processing. *Nat Photonics.* **12**, 534–539 (2018).
26. J. Wang, S. Paesani, Y. Ding, R. Santagati, P. Skrzypczyk, A. Salavrakos, J. Tura, R. Augusiak, L. Mančinska, D. Bacco, D. Bonneau, J. W. Silverstone, Q. Gong, A. Acín, K. Rottwitt, L. K. Oxenløwe, J. L. O'Brien, A. Laing, M. G. Thompson, Multidimensional quantum entanglement with large-scale integrated optics. *Science* **360**, 285–291 (2018).
27. N. H. Wan, T. J. Lu, K. C. Chen, M. P. Walsh, M. E. Trusheim, L. De Santis, E. A. Bersin, I. B. Harris, S. L. Mouradian, I. R. Christen, E. S. Bielejec, D. Englund, Large-scale integration of artificial atoms in hybrid photonic circuits. *Nature* **583**, 226–231 (2020).
28. L. S. Madsen, F. Laudenbach, M. F. Askarani, F. Rortais, T. Vincent, J. F. F. Bulmer, F. M. Miatto, L. Neuhaus, L. G. Helt, M. J. Collins, A. E. Lita, T. Gerrits, S. W. Nam, V. D. Vaidya, M. Menotti, I. Dhand, Z. Vernon, N. Quesada, J. Lavoie, Quantum computational advantage with a programmable photonic processor. *Nature* **606**, 75–81 (2022).
29. W. Liu, M. Li, R. S. Guzzon, E. J. Norberg, J. S. Parker, M. Lu, L. A. Coldren, J. Yao, A fully reconfigurable photonic integrated signal processor. *Nat Photonics.* **10**, 190–195 (2016).
30. D. Pérez-López, A. López, P. DasMahapatra, J. Capmany, Multipurpose self-configuration of programmable photonic circuits. *Nat. Commun.* **11**, 6359 (2020).
31. W. Bogaerts, D. Pérez, J. Capmany, D. A. B. Miller, J. Poon, D. Englund, F. Morichetti, A. Melloni, Programmable photonic circuits. *Nature* **586**, 207–216 (2020).
32. W. Bogaerts, M. Fiers, P. Dumon, Design challenges in silicon photonics. *IEEE J. Sel. Top. Quant. Electron.* **20**, 1–8 (2014).
33. Z. Lu, J. Jhoja, J. Klein, X. Wang, A. Liu, J. Flueckiger, J. Pond, L. Chrostowski, Performance prediction for silicon photonics integrated circuits with layout-dependent correlated manufacturing variability. *Opt. Express* **25**, 9712–9733 (2017).
34. W. Bogaerts, L. Chrostowski, Silicon photonics circuit design: Methods, tools and challenges. *Laser Photon. Rev.* **12**, 1–29 (2018).

Downloaded from https://www.science.org at Stiftung Deutsches Elektronen-Synchrotron on January 23, 2024

35. M. Wuttig, N. Yamada, Phase-change materials for rewriteable data storage. *Nat. Mater.* **6**, 824–832 (2007).
36. B. Gholipour, J. Zhang, K. F. MacDonald, D. W. Hewak, N. I. Zheludev, An all-optical, non-volatile, bidirectional, phase-change meta-switch. *Adv. Mater.* **25**, 3050–3054 (2013).
37. Q. Wang, E. T. F. Rogers, B. Gholipour, C. M. Wang, G. Yuan, J. Teng, N. I. Zheludev, Optically reconfigurable metasurfaces and photonic devices based on phase change materials. *Nat Photonics.* **10**, 60–65 (2016).
38. M. Delaney, I. Zeimpekis, H. Du, X. Yan, M. Banakar, D. J. Thomson, D. W. Hewak, O. L. Muskens, Nonvolatile programmable silicon photonics using an ultralow-loss Sb2Se3 phase change material. *Sci. Adv.* **7**, 1–8 (2021).
39. H. Liu, W. Dong, H. Wang, L. Lu, Q. Ruan, Y. S. Tan, R. E. Simpson, J. K. W. Yang, Rewritable color nanoprints in antimony trisulfide films. *Sci. Adv.* **6**, eabb7171 (2020).
40. K. Chaudhary, M. Tamagnone, X. Yin, C. M. Spägele, S. L. Oscurato, J. Li, C. Persch, R. Li, N. A. Rubin, L. A. Jauregui, K. Watanabe, T. Taniguchi, P. Kim, M. Wuttig, J. H. Edgar, A. Ambrosio, F. Capasso, Polariton nanophotonics using phase-change materials. *Nat. Commun.* **10**, 1–6 (2019).
41. M. Deubel, G. Von Freymann, M. Wegener, S. Pereira, K. Busch, C. M. Soukoulis, Direct laser writing of three-dimensional photonic-crystal templates for telecommunications. *Nat. Mater.* **3**, 444–447 (2004).
42. A. Politi, M. J. Cryan, J. G. Rarity, S. Yu, J. L. O'Brien, Silica-on-silicon waveguide quantum circuits. *Science* **320**, 646–649 (2008).
43. G. D. Marshall, A. Politi, J. C. F. Matthews, P. Dekker, M. Ams, M. J. Withford, J. L. O'Brien, Laser written waveguide photonic quantum circuits. *Opt. Express* **17**, 12546–12554 (2009).
44. B. J. Eggleton, B. Luther-Davies, K. Richardson, Chalcogenide photonics. *Nat Photonics.* **5**, 141–148 (2011).
45. T. Meany, M. Gräfe, R. Heilmann, A. Perez-Leija, S. Gross, M. J. Steel, M. J. Withford, A. Szameit, Laser written circuits for quantum photonics. *Laser Photon Rev.* **9**, 363–384 (2015).
46. O. M. Efimov, L. B. Glebov, K. A. Richardson, E. Van Stryland, T. Cardinal, S. H. Park, M. Couzi, J. L. Brunéel, Waveguide writing in chalcogenide glasses by a train of femtosecond laser pulses. *Opt Mater (Amst).* **17**, 379–386 (2001).
47. A. Zoubir, M. Richardson, C. Rivero, A. Schulte, C. Lopez, K. Richardson, N. Hô, R. Vallée, Direct femtosecond laser writing of waveguides in As_2S_3 thin films. *Opt. Lett.* **29**, 748–750 (2004).
48. M. A. Hughes, W. Yang, D. W. Hewak, Spectral broadening in femtosecond laser written waveguides in chalcogenide glass. *J. Opt. Soc. Am. B.* **26**, 1370 (2009).
49. T. Wu, M. Menarini, Z. Gao, L. Feng, Lithography-free reconfigurable integrated photonic processor. *Nat Photonics* **17**, 710–716 (2023).
50. M. Delaney, I. Zeimpekis, D. Lawson, D. W. Hewak, O. L. Muskens, A new family of ultralow loss reversible phase-change materials for photonic integrated circuits: Sb2S3 and Sb2Se3. *Adv. Funct. Mater.* **30**, 1–10 (2020).
51. C. Ríos, Q. Du, Y. Zhang, C. C. Popescu, M. Y. Shalaginov, P. Miller, C. Roberts, M. Kang, K. A. Richardson, T. Gu, S. A. Vitale, J. Hu, Ultra-compact nonvolatile phase shifter based on electrically reprogrammable transparent phase change materials. *PhotoniX.* **3**, 26 (2022).
52. R. Chen, Z. Fang, J. E. Fröch, P. Xu, J. Zheng, A. Majumdar, Broadband nonvolatile electrically controlled programmable units in silicon photonics. *ACS Photonics.* **9**, 2142–2150 (2022).
53. Z. Fang, R. Chen, J. Zheng, A. I. Khan, K. M. Neilson, S. J. Geiger, D. M. Callahan, M. G. Moebius, A. Saxena, M. E. Chen, C. Rios, J. Hu, E. Pop, A. Majumdar, Ultra-low-energy programmable non-volatile silicon photonics based on phase-change materials with graphene heaters. *Nat. Nanotechnol.* **17**, 842–848 (2022).
54. J. Chan, G. Hendry, K. Bergman, L. P. Carloni, Physical-layer modeling and system-level design of chip-scale photonic interconnection networks. *IEEE Trans. Comput.-Aided Des. Integ. Circuits Syst.* **30**, 1507–1520 (2011).
55. S. Ohno, R. Tang, K. Toprasertpong, S. Takagi, M. Takenaka, Si microring resonator crossbar array for on-chip inference and training of the optical neural network. *ACS Photonics.* **9**, 2614–2622 (2022).
56. C. Wu, H. Yu, S. Lee, R. Peng, I. Takeuchi, M. Li, Programmable phase-change metasurfaces on waveguides for multimode photonic convolutional neural network. *Nat. Commun.* **12**, 96 (2021).
57. J. Feldmann, N. Youngblood, M. Karpov, H. Gehring, X. Li, M. Stappers, M. Le Gallo, X. Fu, A. Lukashchuk, A. S. Raja, J. Liu, C. D. Wright, A. Sebastian, T. J. Kippenberg, W. H. P. Pernice, H. Bhaskaran, Parallel convolutional processing using an integrated photonic tensor core. *Nature* **589**, 52–58 (2021).
58. L. Zhuang, C. G. H. Roeloffzen, M. Hoekman, K.-J. Boller, A. J. Lowery, Programmable photonic signal processor chip for radiofrequency applications. *Optica.* **2**, 854–859 (2015).
59. D. Pérez, I. Gasulla, L. Crudgington, D. J. Thomson, A. Z. Khokhar, K. Li, W. Cao, G. Z. Mashanovich, J. Capmany, Multipurpose silicon photonics signal processor core. *Nat. Commun.* **8**, 1–9 (2017).
60. O. Daulay, G. Liu, K. Ye, R. Botter, Y. Klaver, Q. Tan, H. Yu, M. Hoekman, E. Klein, C. Roeloffzen, Y. Liu, D. Marpaung, Ultrahigh dynamic range and low noise figure programmable integrated microwave photonic filter. *Nat. Commun.* **13**, 1–8 (2022).
61. R. A. Cohen, O. Amrani, S. Ruschin, Response shaping with a silicon ring resonator via double injection. *Nat Photonics.* **12**, 706–712 (2018).
62. S. Pai, Z. Sun, T. W. Hughes, T. Park, B. Bartlett, I. A. D. Williamson, M. Minkov, M. Milanizadeh, N. Abebe, F. Morichetti, A. Melloni, S. Fan, O. Solgaard, D. A. B. Miller, Experimentally realized in situ backpropagation for deep learning in nanophotonic neural networks. *Science* **380**, 398–404 (2023).
63. C. Rios, M. Stegmaier, P. Hosseini, D. Wang, T. Scherer, C. D. Wright, H. Bhaskaran, W. H. P. Pernice, Integrated all-photonic non-volatile multi-level memory. *Nat Photonics.* **9**, 725–732 (2015).
64. Z. Cheng, C. Ríos, W. H. P. Pernice, C. David Wright, H. Bhaskaran, On-chip photonic synapse. *Sci. Adv.* **3**, e1700160 (2017).
65. C. Ríos, Y. Zhang, M. Y. Shalaginov, S. Deckoff-Jones, H. Wang, S. An, H. Zhang, M. Kang, K. A. Richardson, C. Roberts, Multi-level electro-thermal switching of optical phase-change materials using graphene. *Adv Photonics Res.* **2**, 2000034 (2021).

Acknowledgments

Funding: C.W., H.D., and M.L. acknowledge the funding support provided by ONR MURI (award no. N00014-17-1-2661) and the NSF (award no. CCF-2105972). Y.-S.H., H.Y., I.T., and C.A.R.O. acknowledge the funding support by NSF (award no. ECCS-2210168 and DMR-2329087). Part of this work was conducted at the Washington Nanofabrication Facility/Molecular Analysis Facility, a National Nanotechnology Coordinated Infrastructure (NNCI) site at the University of Washington with partial support from the NSF via awards NNCI-1542101 and NNCI-2025489. **Author contributions:** M.L. and C.W. conceived the research and designed the experiments. C.W. and H.D. designed and fabricated the photonic devices and performed the experiments. H.Y., Y.-S.H., C.A.R.O., and I.T. developed and deposited the Sb_2Se_3 thin film. C.W., H.D., and M.L. analyzed the data. C.W. and M.L. wrote the manuscript with contributions from all the authors. All authors discussed the results and commented on the manuscript. **Competing interests:** M.L., C.W., and H.D. filed a US Provisional Patent Application (no.: 63/516,267) titled "Freeform direct-write and rewritable photonic circuits on phase-change thin layers" with the US Patent and Trademark Office (USPTO) on 28 July 2023. The authors declare no other competing interests. **Data and materials availability:** All data needed to evaluate the conclusions in the paper are present in the paper and/or the Supplementary Materials.

Submitted 4 August 2023
Accepted 1 December 2023
Published 5 January 2024
10.1126/sciadv.adk1361

Downloaded from https://www.science.org at Stiftung Deutsches Elektronen-Synchrotron on January 23, 2024